JOURNAL OF MATERIALS SCIENCE **36** (2001) 4851–4862

Influence of powder characteristics and powder processing routes on microstructure and properties of hot pressed silicon nitride materials

A. BONDANINI, F. MONTEVERDE, A. BELLOSI
IRTEC-CNR, Research Institute for Ceramics Technology, Via Granarolo 64, 48018 Faenza, Italy
E-mail: bellosi@irtec1.irtec.bo.cnr.it

Four different commercial Si_3N_4 powders were hot pressed with the addition of La_2O_3 and Y_2O_3 as sintering aids. Two powder processing routes were set up: addition of sintering aid powders by ultrasonic dispersion, addition of nanodispersed amorphous additive species by chemical coprecipitation. The following aspects were analyzed: characteristics of starting powders and powder mixtures, with reference to surface modification (electrokinetic behaviour and surface properties) induced by the powder treatment; sintering behaviour of the powder mixtures; influence of raw powders characteristics and processing route on microstructure and properties of dense materials. The microstructural characteristics of hot pressed materials (grain size, aspect ratio, grain boundary phases) were found to be dependent on powder characteristics and its process history. Significant variation of the mechanical properties (Young modulus, hardness, toughness and strength) were related to microstructural features. Strength, for example, ranges from 600 to 1200 MPa at room temperature and from 400 to 1000 MPa at 1200°C; toughness ranges from about 4 to about 6 $MPam^{1/2}$.

1. Introduction

The combination of mechanical, chemical, physical properties makes silicon nitride a material suitable for high performance structural applications. Dense Si_3N_4-based materials can be fabricated by the use of additives that promote liquid phase sintering. However, the presence of a liquid medium implies the formation of intergranular phases that influence all the properties, depending on their composition, amount and distribution. In order to improve properties, much research is focused on the control of the resulting microstructure (grain size and shape, flaws, characteristics of intergranular phases) through the production of fine and pure powders, the design of sintering aid systems and the development of controlled powder processing and densification procedures [1–10].

The addition of sintering aids is a crucial step in the production process [3, 4], as inhomogeneities introduced at this stage remain inside the material. Generally the processing of powders modifies their surface characteristics, reduces the particle size, determines the distribution of the sintering aids and influences the interparticle interactions. If the additive is a powder, the finite size of the particles may cause difficulties for intimate mixing. Considerable advantages can be gained using chemical methods to produce additives in a finely divided form or to distribute them homogeneously in a nanoscale on the silicon nitride surface. This technique can provide an excellent control of the distribution and the microchemistry of intergranular phases [4, 5, 11–16], but the relationships between processing and properties still need to be further investigated, particularly regarding high temperature properties and reliability. Actually, in some cases, the chemical processes are expensive and may act as a technological barrier in view of their scale-up to industrial mass production.

The present investigation aims to assess the role of the powder characteristics and treatments on sintering behaviour of the final powder mixtures and on microstructure and mechanical properties of dense hot pressed materials. For this purpose, four different commercial Si_3N_4 powders and two different powder processing routes were tested: (i) ultrasonic mixing: a clean, fast, cheap, reliable method; (ii) chemical coprecipitation from nitrates: a more complex and expensive procedure with enhanced potentialities but technological limitations. Sintering aids were chosen in the system $La_2O_3 + Y_2O_3$, as they result in high solidus temperature and viscosity, originating refractory phases on crystallisation.

2. Experimental details

Four commercial powders were selected on the basis of their production process: nitridation of silicon and grinding: P95H (Kemanord, Sweden) and M11 (H.C. Starck, Germany) named powders P and M, respectively; chemical synthesis by liquid/vapour

phase: SNE-10 (UBE, Japan) and Baysinid ST (Bayer, Germany) named powders U and B, respectively.

Two starting compositions were designed (amounts in wt%):

$96Si_3N_4 + 2La_2O_3 + 2Y_2O_3$ (composition 1)
$94Si_3N_4 + 3La_2O_3 + 3Y_2O_3$ (composition 2)

The techniques used to add the sintering aids were the followings:

- *Ultrasonic mixing*: Stirring of separate dispersion of Si_3N_4 and additive powders: La_2O_3 (Merck) and Y_2O_3 (Starck) in water by ultrasonic pulses, then mixing of the two dispersions under magnetic stirring at pH 10, adjusted with concentrated NH_3. A subsequent ultrasonic mixing by pulsed cycles was performed for a total time of 10 min. The mixture was freeze dried and sieved.
- *Chemical coprecipitation from nitrate solutions*: Separate ultrasonic stirring in water of Si_3N_4 powder and of Y- and La-nitrates ($Y(NO_3)_3 \cdot 6H_2O$, $La(NO_3)_3 \cdot 6H_2O$), mixing of the two dispersion under controlled pH 9.5–10.5 by use of $(Et)_4NOH$, in order to allow metal hydroxides precipitation on Si_3N_4 particles surface. After three stages of sedimentation and washing with $(Et)_4NOH$ water solutions (pH 10), the mix was freeze dried and calcined at 400°C for 1 hour under flowing N_2 gas.

Characteristics of the starting Si_3N_4 powders and dried powder mixtures are summarized, respectively, in Tables I, II and III. Oxygen content was measured by LECO analyzer; the content of other impurities is based on manufacturer specifications. Specific surface area (s.s.a.) was measured by three-point B.E.T. method. The value of equivalent spherical diameter was calculated by specific surface area, the mean dimensions of particles and/or aggregates ($D_{10,50,90}$) were estimated by cumulative mass% curves obtained with X-ray Sedimentation analyzer.

Z-potential values and pH_{IEP} (pH of the isoelectric point) of starting and processed powders were determined by Electrokinetic Sonic Amplitude (ESA) measurements, in a 350 cm^2 Teflon measure cell attached to the electroacustic analysis system, at 25°C, using 1 vol% suspensions. The Acousto Sizer was equipped with a microliter autotitrator, an overhead glass mixer that provides a continuous stirring during measurements and probes for pH, temperature and conductivity measurements. The ESA potentiometric titrations were carried out separately in the basic and acidic direction. The pH was set with 1 M KCl and 1 M NaOH. KCl was used to adjust a constant ionic strength ($I = 10^{-2}$ M) and was added prior to the mixing process. Previous studies have shown that K^+, Na^+, $C1^-$ behave as indifferent electrolytes for Si_3N_4 and the adopted conditions did not affect the z-potential measurements [17–21].

Morphology and distribution of raw and mixed powders were analysed by SEM. Their crystallinity was estimated by standard powder X-ray diffraction (XRD). Atomic ratios of surface elements, on raw Si_3N_4 powders and final mixtures of composition 2, were measured by X-ray photoelectron spectra (XPS) analyses, according to a procedure described in previous works [19, 21].

All the mixtures were hot pressed under vacuum in a BN-lined induction heated graphite die using a pressure of 30 MPa and a temperature of 1850°C. Continuous shrinkage of the samples was recorded during hot pressing. Using a SEM equipped with a backscattered electron detector, microstructure of dense materials was examined on fractured and polished-plasma etched surfaces, parallel and perpendicular to the applied pressure. Mean grain size and aspect ratio of elongated β-Si_3N_4 were estimated. Crystalline phases of dense materials as well as an orientation degree (intensity ratio of the reflections (200) over (002) of the β-Si_3N_4 grains) were analyzed by XRD. In order to evaluate the recrystallization of the residual secondary phases, annealing tests were performed on some samples at 1400°C for 6 hours in a flowing nitrogen atmosphere.

Young's modulus (E) was measured on ($0.8 \times 8.0 \times 28.0$) mm^3 plate, using the frequency resonance method [22]. Flexural strength (σ) was measured on ($2.00 \times 2.50 \times 25.00$) mm^3 chamfered bars, in a 4-pt bending fixture (20 mm outer span, 10 mm inner span, crosshead displacement of 0.5 mm/min) at room

TABLE II Characteristics of the starting powders

		Atomic ratios			Estimated surface sites (%)		
Powder	pH_{IEP}	N/Si	Si/O	N/O	Si_2N_2O	Si_3N_4	SiO_2
U	6.6	1.0	2.2	2.2	100	–	–
B	4.0	.75	1.1	.8	–	52	48
P	5.1	1.5	0.5	.8	–	59	41
M	7.1	1.1	3.9	4.2	–	87	13

pH_{IEP}: isoelectric point (ESA analyses), atomic ratios of surface elements (XPS analyses), surface species evaluated by XPS data (according to the procedure described in Ref. 14)

TABLE I Characteristics of the starting powders

							Impurities (wt%)					
Powder	$\alpha/(\alpha+\beta)$ Si_3N_4	s.s.a (m^2g^{-1})	d (μm)	D_{10} (μm)	D_{50} (μm)	D_{90} (μm)	O	C	Cl	Fe	Ca	Al
U	.95	11.5	0.16	0.27	0.51	0.92	1.09	–	0.01	0.01	0.005	0.005
B	.94	12.2	0.15	0.23	0.57	1.2	1.44	–	0.1	0.005	0.0003	0.0003
P	.93	7.3	0.26	0.23	0.77	4.0	1.35	0.29	–	0.06	0.01	0.03
M	.90	11.6	0.16	0.21	0.54	3	0.81	0.2	–	0.01	0.01	0.08

α/β ratio of the two Si_3N_4 crystalline phases; s.s.a.: specific surface area (BET); d: equivalent spherical diameter; D: particle aggregates size corresponding to 10, 50, 90 cumulative wt% of the granulometric distribution (Sedigraph); oxygen amount (LECO); other impurities (from the powder suppliers).

TABLE III Characteristics of the powder mixtures

Material	2 Uu	2 Uc	1 Uu	1 Uc	1 Bu	1 Bc	1 Pu	1 Pc	1 Mu	1 Mc
s.s.a. (m^2/g)	11.9	10.9	11.0	12.5	10.5	10.7	8.6	9.0	16.3	13.0
O wt%	3.4	4.2	1.76	2.23	2.23	2.48	2.09	2.27	1.61	2.22
ΔO wt.%	(+2.31)	(+3.11)	(+0.67)	(+1.14)	(+0.79)	(+1.04)	(+0.74)	(+0.92)	(+0.8)	(+1.41)
pH_{IEP}	8.1	8.7		10.9		10.5		8.9		9.4
ΔpH_{IEP}	(+1.5)	(+2.2)		(+4.2)		(+6.1)		(+3.6)		(+2.2)
ΔI_{EP} to 11.1[a]				0.22		0.61		2.18		1.73
Y/Si	0.02	0.30								
La/Si	0.007	0.20								

u: mixtures from ultrasonic mixing; c: mixtures from chemical coprecipitation; s.s.a.: specific surface area (BET); O: oxygen content (LECO); ΔO: increase in oxygen content after coprecipitation, in respect with oxygen content in the starting powders; pH_{IEP}: pH of the isoelectric point (ESA), ΔpH_{IEP}: variation of the isoelectric point in the coprecipitated mixtures in respect with the starting powders, ΔpH_{IEP} to 11.1[a] (difference in the isoelectric points of the mixture and of the additives); Y/Si and La/Si: atomic ratios (XPS analyses).
[a]Mean value of pH_{IEP} of the additives.

temperature up to 1400°C in laboratory air. Vicker's microhardness (HV 1.0) was measured with the Zwick hardness tester on polished surfaces with a load of 9.81 N. Fracture toughness (K_{IC}) was evaluated with the direct crack measurement (DCM) method with a load of 98.1 N in the same tester using the formula proposed by Anstis *et al*. [23]. Crack propagation was then observed by SEM on polished-etched surfaces.

3. Results and discussion

3.1. Starting Si_3N_4 powders

The characteristics of raw Si_3N_4 powders are shown in Tables I and II. Among the tested powders U, B and M present approximately the same specific surface area, higher than P. Powders M and P are characterised by relatively wide particle size distribution and irregularly shaped (mainly acicular) particles. On the other hand, powders U and B have spherical particle shape and narrow particle size distributions. Type and amount of impurities depend on the synthesis route: apart from oxygen, which amount is low in powder M, the content of the other impurities is about two orders of magnitude higher in powders (P and M) produced by nitridation of silicon than in powders (U and B) produced by chemical synthesis. The presence of oxygen is due to a partial surface oxidation of powder particles, because of the thermodynamic instability of silicon nitride in air. Therefore, the particle surface is covered by a layer containing mainly amphoteric silanol (Si−OH), basic secondary amine groups (Si_2=NH), and silicon oxynitride (Si_2N_2O), in different amounts, depending on powder preparation and subsequent treatments. According to the atomic ratios measured by XPS (Table II), powder U seems to present an homogeneous and complete surface layer composed by Si_2N_2O. In powder P and B two distinct XPS silicon peaks were detected and attributed to Si_3N_4 and SiO_2, surface sites that accounts for the presence of a probably patchwise oxygen-rich surface [19]. Type and estimated amounts of surface sites in the different Si_3N_4 powder particles are indicated in Table II. Presumably, as reported specifically for silica samples [24], several different kinds of Si−O species are present at the surface, these including also Si-OH bonds. Powder M presents this dual composition too, but with a low percentage of SiO_2 sites (Table II) confirming the low oxygen content detected by LECO technique. XPS analyses revealed also the presence of fluorine, due to chemical leaching on powder M in order to reduce surface silica. The results relative to powder M are in agreement with previous studies of silicon nitride powders produced by nitridation of silicon [25, 26].

The presence of these surface species on Si_3N_4 particles are confirmed by the values of the pH_{IEP} measured by ESA analyses (Fig. 1). The shift of the pH_{IEP} values is due to differences of surface oxygen content: (i) a more acid surface derived from a larger presence of surface silica sites (or a mixture of silica and silicon nitride) for powder P and B [19–21, 27], (ii) a more basic surface due to oxynitride film coating in powder U; (iii) a surface mainly covered by basic silylamine groups for M. In addition, looking at the curves in Fig. 1, it is possible to confirm the presence of these surface sites (Table II). In correspondence of strongly acid pH, the z-potential results positive, proportionally to the presence of silylamine positive groups ($Si{=}NH_2^+$), besides neutral Si-OH groups, this effect being particularly evident for powder M. Instead, the values of z-potential in basic pH is negative due to the couple SiO/Si=NH and in this case powders B and P seem to be richer in silanol groups. Powder U shows an intermediate behaviour due to a composition neither silanolic nor silylaminic. The chemistry of coating layers drives the particles' reactivity: oxynitride sites seem to be more reactive than silanol/silylamine ones.

The surface status of silicon nitride powders undergoes modification depending on processing routes. It was ascertained [19] that also powder U, which has a more homogeneous and slightly oxidized surface, after attrition milling, ultrasonic mixing and ball milling, presents increasing amount of SiO_2, in a direct relationship with processing time. Among the mentioned processing routes, ultrasonic mixing changes the surface characteristics less than the other methods. Therefore, in the present study, it was chosen as a route alternative to chemical methods for the addition of sintering aids to silicon nitride powders.

3.2. Powder mixtures

The introduction of sintering aids involves several interactions (such as heterocoagulation, precipitation, segregation) between silicon nitride and additive particles; these phenomena are strongly dependent on the surface

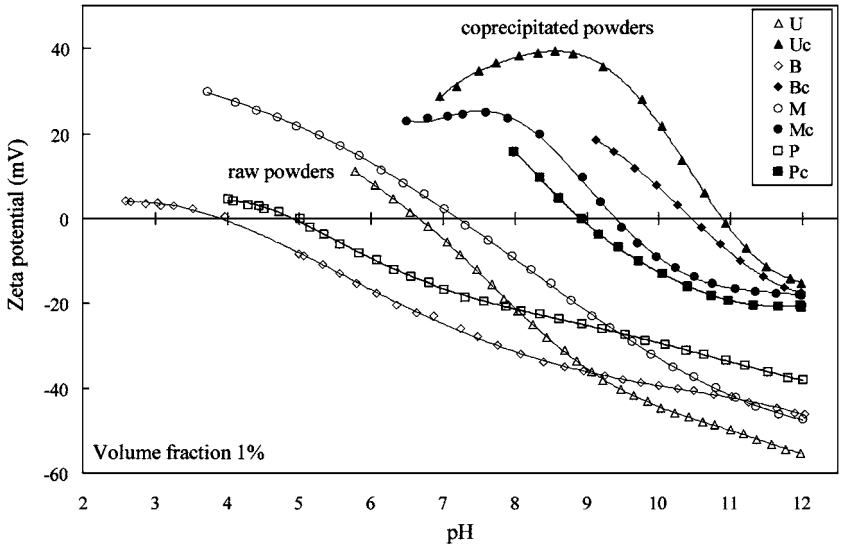

Figure 1 ESA titration curves of the four raw silicon nitride powders and the four mixtures containing the additives (2 wt% $La_2O_3 + 2$ wt% Y_2O_3) introduced through chemical coprecipitation (c).

properties of the starting powders. Particle surface characteristics influence the dispersing behaviour of the suspensions during the addition of sintering aids, as the specific adsorption of the metal ions influences the solid-liquid interface properties. The two metal oxides Y_2O_3 and La_2O_3 used as sintering aids present basic surfaces, pH_{IEP} 10.4 and 11.8 respectively, and their minimal solubilities were calculated to correspond to pH 10.2 and 9.8 [19]. Considering that the four silicon nitride powders have a more acidic surface than the two sintering aids, heterocoagulation occurs in the opposite z-potential overlapping pH range, where the additive and Si_3N_4 particles exhibit opposite surface charges. Moreover, in chemical coprecipitation method, an additional phenomenon of nucleation and growth (precipitation of mainly amorphous nuclei of metal oxide species) should occur in the pH range corresponding to the minimal solubility of the additives. On these basis, regardless of the mixing process, experimental pH for the addition of the oxides was strictly maintained in the range 9.5–10.5, in order to fit with the condition of minimal solubility of Y- and La-oxides and to fall into the pH range of opposite z potential values. Relationship among phenomena occurring during the addition of sintering aids (heterocoagulation and/or precipitation), surface properties and type of resulting coating are still open arguments to be further investigated [20].

3.2.1. Ultrasonic processing effects

The ultrasonic dispersion acts exclusively through heterocoagulation of silicon nitride and additive powders and it limits the contamination that usually derives from milling media and allows homogenization of the powders in a very short time. Electroacoustic analyses [20, 21] showed that a good "coating" of the silicon nitride particle surface with additive species can be obtained with ultrasonic dispersion, the experimental atomic ratios La/Si and Y/Si approximating the theoretical values [19] (Table III). The preferential surface enrichment of yttria in respect to lanthania is due to its higher positive z-potential at the selected experimental pH values. SEM analyses indicated the presence of randomly distributed aggregates of additives with dimensions lower than 3 μm.

3.2.2. Coprecipitation

Comparing the relative ESA titration curves (Fig. 1) of all the coprecipitated mixtures with composition 1, the following features can be highlighted: (i) the pH_{IEP} shifts towards basic values, i.e. towards those of the additive oxides; pH_{IEP} values of the mixtures close to those of the additives indicate a homogeneous coating without segregation of precipitated hydroxides; the Si_3N_4 particle surface behaves as a surface coated with $Y(OH)_3$ and $La(OH)_3$; (ii) the difference in the pH_{IEP} values between the starting silicon nitride powder and the relative mixtures (Table III) gives an estimation of the heterocoagulation and coprecipitation processes and a relative comparison of the raw powder surface reactivity.

The experimental atomic ratios (Y/Si and La/Si) revealed by XPS analyses (the data in Table III are relative to mixture 2U) appear to be at least one order of magnitude larger in coprecipitated powders than in ultrasonicated ones, owing to the additional coprecipitation phenomenon. As in the previous case, the surfaces are richer of Y than of La, due to better specific adsorption (heterocoagulation) of Y_2O_3 than La_2O_3 for the reasons above explained.

It is possible to establish a merit rating concerning the surface reactivity of each silicon nitride powder, in respect with an ideal configuration:

- *Powder B*: It exhibits a surface composed mainly of silica that favours a large number of nucleation sites scarcely reactive; it implies a weak but homogenous growth of additive species which induces the formation of a film with a high screening effect in respect to the substrate, as suggested by the high ΔpH_{IEP}.
- *Powder U*: The homogeneous surface layer of Si_2N_2O on particles of powder U gives rise a rapid

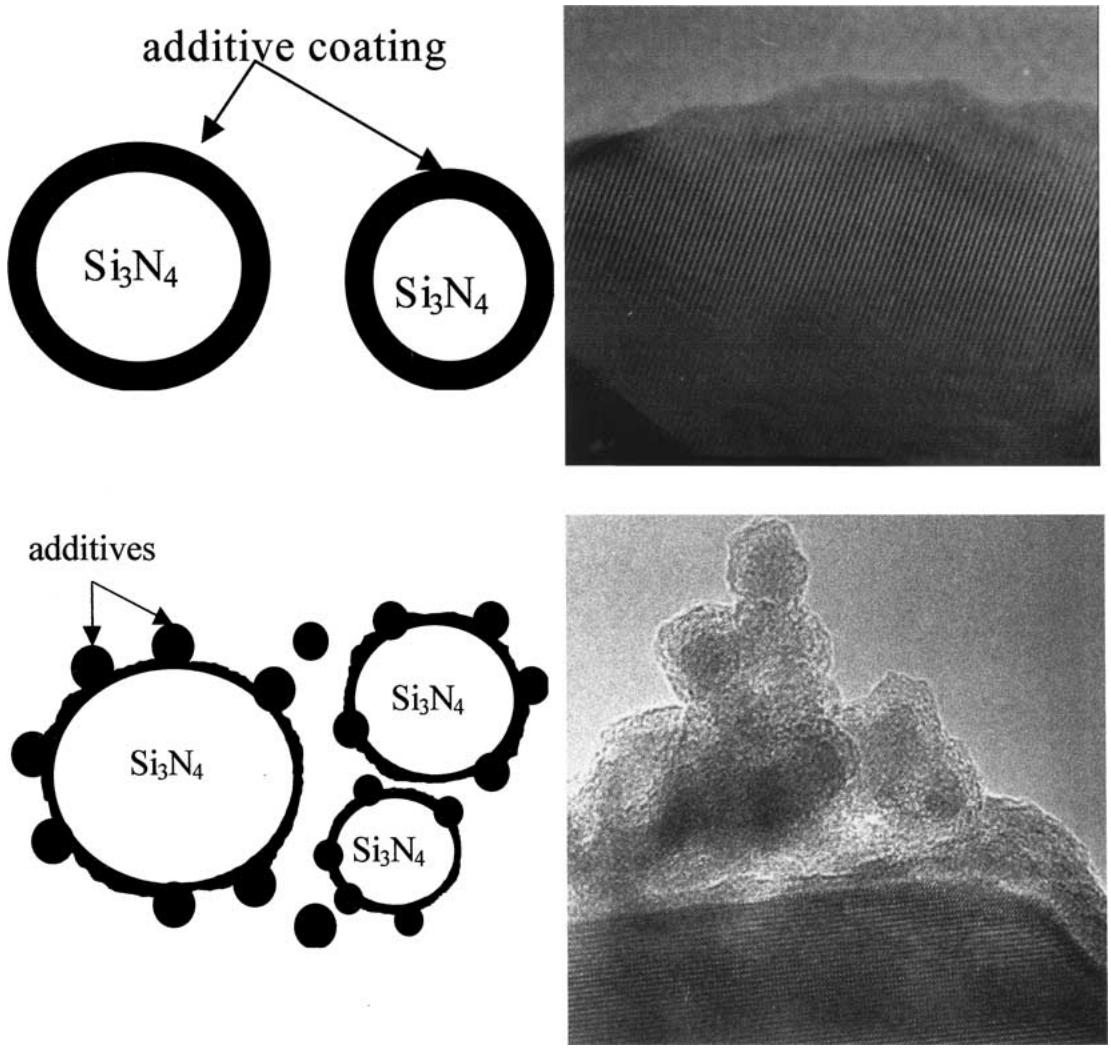

Figure 2 Scheme of the distribution of the additives around the silicon nitride powder particles: (a) homogeneous coating of amorphous additive species as observed on powder U and (b) formation of nanoclustered amorphous additive species, observed on powder P.

nucleation of Y and La oxides with few nuclei but a large growth that provides a smooth coating. The morphology and smoothness of this coating was observed by TEM analyses (Fig. 2a).

– *Powder P*: Features like high surface concentration of silanol groups with low initial reactivity, large grain size distribution, low specific surface area and irregular particle shape favour inhomogeneous heterocoagulation of the additive species on particle surface that results in the worst screening effect in respect to the substrate.
– *Powder M*: The low content of silanol groups and the presence of sylilamine imply a scarce surface reactivity, that causes a minimal heterocoagulation of the additive species and inhomogeneous surface coating of Si_3N_4 powder particles.

Concerning powders P and M, it can be hypothesized that amorphous clusters of additive precipitates form, consisting of clumps of nanosized, near round shaped particles, which are supposed to be the first cause of the observed increase in specific surface area (Tables I and III and Fig. 2b).

As crystalline phases, peaks due to additive phases (La_2O_3, Y_2O_3 and some $La(OH)_3$) were detected in the mixed powders. In addition, the coprecipitated powders present always an higher oxygen content than the ultrasonicated ones, owing to the calcination step (Table III).

The results confirm that morphology and distribution of the additive-containing coating on the surface of the core particles depend on precipitation and heterocoagulation mechanisms, which are related to surface charge characteristics, particle surface chemistry, size and distribution of core and precipitated particles, amount of the additive precursors (i.e. concentration of metal ions), nature of the other ion species in solution, kinetics of precipitation, pH, viscosity) [16–21, 28, 29]: their influence is not yet completely clear and the optimization of the chemical processes needs to be further investigated.

3.3. Densification behaviour during hot pressing

The sintering behaviour of the powder mixtures during hot pressing under constant experimental conditions ($T = 1850°C$, $P = 30$ MPa) are compared in Fig. 3a and b, where the relative density is reported vs. the temperature from the onset of shrinkage up to 1850°C, and vs. time during the isothermal step at 1850°C. The relative densitiy values were calculated from the shrinkage curves recorded during the hot pressing.

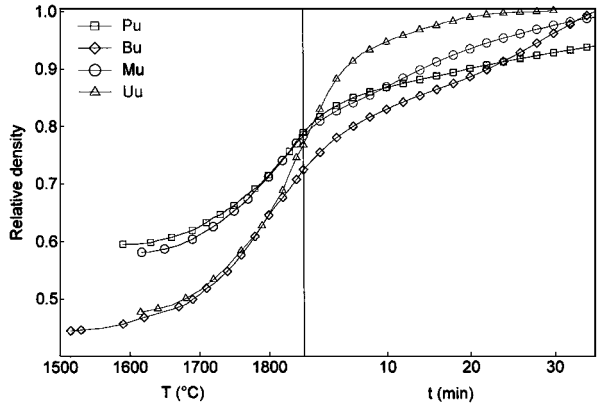

(a)

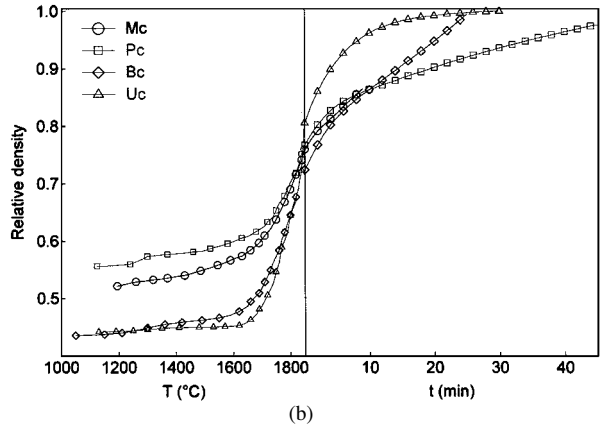

(b)

Figure 3 Densification behaviour during hot pressing, vs. temperature up to 1850°C and vs. time during the isothermal stage. (a) mixtures after ultrasonic mixing: u; (b) mixtures after coprecipitation: c.

The green densities are 2–5% higher in the ultrasonicated powders than in the coprecipitated ones, due to the presence, in the latter case, of coatings or nanoprecipitates that lower the flowability of the particles. Under constant powder treatment, the powders produced by nitridation of silicon (P and M) have a green density 10–15% higher than powders from chemical synthesis (U and B). It has to be related to particle size distribution and particle shape: narrow grain size distribution and round shape (as in powders U and B) lower the green density.

The temperature (as registered during hot press run) at which the shrinkage starts (T_0, Table IV) indicates the outset of the first densification stage (particle rearrangement and fragmentation) and ranges from ∼1500 to ∼1650°C for ultrasonicated mixtures and from ∼1050 to ∼1200°C for chemically coprecipitated powders. The unusual behaviour observed in the latter case (i.e. the start of shrinkage at relatively low temperatures and the very slow shrinkage up to the temperature correspondent to the initial densification of ultrasonicated powders) is related to the morphology and distribution of the additives, in the form of particle coatings or clumps of nanosized precipitates. As in this stage densification is presumed to be due to the flux of matter through the contact regions to the surface of the necks between solid particles, the presence of fine additive precipitates may have undergone slow fragmentation under stress, and consequently to a slow flux to the pores at the edges of the Si_3N_4 particle surfaces, until the system reaches a fractional volume of porosity equivalent to that of powders from ultrasonic dispersion [4].

TABLE IV Values of the relative density

Sample[a]	ρ_0 (%)	ρ_{1850} (%)	ρ_f (gr/cm^3)%		T_0 (°C)	T_{liq} (°C)
1 Uc	44.2	80.1	3.26	100	1130	1700
1 Uu	47.7	76.7	3.25	100	1615	1730
1 Bc	43.6	72.5	3.22	99.5	1050	1650
1 Bu	44.4	72.4	3.23	99.9	1515	1650
1 Pc	55.6	76.7	3.16	97.7	1125	1530
1 Pu	59.5	78.9	3.04	93.8	1590	1630
1 Mc	52.2	76.0	3.24	99.9	1195	1560
1 Mu	58.1	78.3	3.20	98.9	1615	1670
2 Uc	44.0	90.0	3.28	100	1100	1750
2 Uu	47.5	85.0	3.27	100	1640	1740

ρ_0: green density; ρ_{1850} at 1850°C, ρ_f: final density; T_0: temperature of shrinkage onset; T_{liq}: temperature at which starts the second densification stage.

[a]u: mixtures from ultrasonic mixing; c: mixtures from chemical coprecipitation.

At the same time, when large amount of liquid is formed, the solution-diffusion-reprecipitation mechanism drives the densification in the second stage at a rate depending on composition and viscosity of the liquid medium. The temperature at which the second densification stage starts corresponds approximately to the liquidus temperature (T_{liq} in Table IV) and ranges from ∼1530 to ∼1750°C. Both these temperatures and the densification rates are dependent on:

- *Type and amount of the additives*. The high temperatures required to densify these powder mixtures depend mainly on the selected additives. The liquidus temperatures measured for the mixtures from powder U are in agreement with the Y_2O_3-La_2O_3 [30] and Y_2O_3-La_2O_3-SiO_2 [31] phase diagrams. The variation in the liquidus temperature observed for the different samples are to be ascribed to oxygen and impurities in the starting powders, as described below. At constant powder treatment, an higher amount of additives (of the same composition) increases T_{liq}, because of the lower influence of impurities and oxygen present in the starting powders on liquidus composition.
- *Starting powder characteristics*. The values of T_{liq} are relatively lower in samples produced from powders P and M, due to the amount (three orders of magnitude higher than in powders U and B) of impurities like Ca, Fe and Al which contribute to decrease the liquidus eutectic and to increase the amount of liquid. Secondarily, also oxygen content affects the liquidus temperature and it can be the reason of the difference in T_{liq} between the two pure powders U and B.
- *Powder treatment methods*. In the case of powders U and B, powder treatments slightly affect T_{liq}. On the contrary, this effect is remarkable when using powders P and M. In all the cases, the cause of the lower liquidus temperature in chemically processed than in ultrasonicated powder mixtures is the association of their relatively higher amount of oxygen with metal impurities.

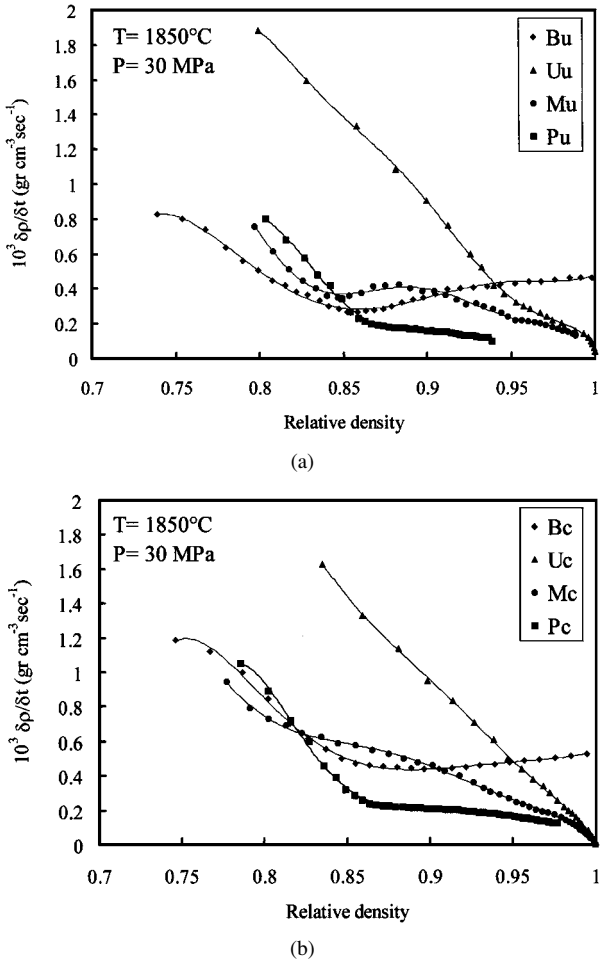

Figure 4 Densification rate vs. relative density during the isothermal stage. (a) mixtures after ultrasonic processing: u and (b) mixtures after chemical coprecipitation: c.

During heating up to 1850°C, samples from composition 2 (more additives and, consequently, liquid phase) reached relative densities higher than 85%, while for composition 1 the relative densities range from 72 to 80%. Under constant hot pressing conditions, i.e. during the soaking time at 1850°C, the sintering behaviour is strongly dependent on the starting powders. The plots reporting the densification rates against relative density (Fig. 4a and b) during isothermal treatment show the following main features:

- Mixtures from powder U reveal a linear decrease of the densification rate, with a relatively high slope, particularly up to 95% of relative density (i.e. regarding the 2nd densification stage), and the slope decrease when the 3rd densification stage (elimination of closed porosity) becomes active.
- In the case of the mixtures from the other powders, the densification rate is lower and decreases approximately linearly up to about 85% of relative density. Afterwards, powder P has a low and nearly constant densification rate, which does not allow to obtain full dense samples (relative densities 93–97%). In mixture from powder M, the densification rate decreases slowly, nevertheless nearly full density is achieved (about 99%). In both these cases the large grain size distribution of the particles induces inhomogeneous sinterability, i.e. hinders densification mechanisms where larger particles are present as they influence liquid phase sintering kinetics [32]. In addition, due to the low purity of these powders, as above described, the local composition and distribution of liquid phase during sintering is not homogeneous.
- The unusual behaviour observed for the mixtures from powder B (after a decrease of densification rate, it seems that densification rate increases) is related to a partial surface decomposition of silicon nitride that is registered during hot pressing after the sample reaches 85% of relative density, and observed in the hot pressed samples. This feature is still unclear because the powder possesses all the characteristics for an excellent sinterability (high purity, narrow grain size distribution and round particle shape). Similar decomposition was not revealed using the other silicon nitride powders.

To conclude, powder U demonstrated the best sinterability, owing to a unique combination of characteristics: the narrowest size distribution, round shape particles, high reactivity, most homogenous surface covering of additives.

4. Microstructure of hot pressed materials

SEM micrographs on plasma etched surfaces compare the microstructural features of hot pressed materials changing either silicon nitride powders (Fig. 5a–d) or processing route (Fig. 6a and b). Typical microstructural parameters (final density, orientation degree, residual α-Si_3N_4 and grain size) are reported in Table V.

The microstructure presents in any case elongated grains mixed with smaller and equiaxed grains, although these features change in the various sintered materials. In fact, the microstructural evolution depends on the mechanisms, involved during densification/grain growth processes, that are related to the powder processing history. It is well known that during densification and $\alpha \rightarrow \beta$-Si_3N_4 phase transformation, β-Si_3N_4 nuclei form with crystallographic orientation, initiating the growth of primary rod-like β phase, having the basal planes parallel to the direction of the applied pressure. Number, size and growth rate of the β phase are governed by key factors such as type, distribution of the liquid phase and the characteristics of powder mixtures. Consequently, hot pressed materials studied in this work present different amounts of elongated grains in respect of regularly shaped grains, mean grain size, aspect ratio of the elongated grains, microstructure anisotropy parallel and perpendicular to the applied pressure, porosity and defects. Residual α-Si_3N_4 was detected only in samples from powder U: due to refractoriness of the liquid phase (see liquidus temperature), the solubility of α-Si_3N_4 was limited. A pronounced orientation of β-Si_3N_4 grains, indicated by the low value of I_{200}/I_{002} (Table V), was assessed by X-Ray diffraction in all the sintered samples, with the basal planes aligned to the direction parallel to that of the applied pressure. Such a feature is confirmed by the typical morphology observed upon the surfaces parallel and perpendicular to the pressing direction

TABLE V Some microstructural parameters of the hot pressed materials

Sample	ρ (gr/cm^3)	ρ (%)	Residual α-Si_3N_4 (vol%)	I_{200}/I_{002}(*) β-Si_3N_4	D (μm)	a
1 Uc	3.26	100	15	1.5	0.45 ± 0.1	7.0 ± 2.4
1 Uu	3.25	100	Traces	2.5	0.4 ± 0.1	7.8 ± 1.9
1 Bc	3.22	99.5	0	0.7	0.5 ± 0.2	6.1 ± 2.4
1 Bu	3.23	99.9	0	1.6	0.6 ± 0.2	6.5 ± 2.0
1 Pc	3.16	97.7	0	1.8	0.7 ± 0.2	5.4 ± 1.9
1 Pu	3.04	93.8	0	1.8	0.7 ± 0.3	5.7 ± 1.8
1 Mc	3.24	99.9	0	2.1	0.6 ± 0.25	6.0 ± 2.1
1 Mu	3.20	98.9	0	0.9	0.6 ± 0.2	7.3 ± 2.6
2 Uc	3.28	100	15	1.9	0.4 ± 0.05	9.8 ± 2.0
2 Uu	3.27	100	9	2.2	0.35 ± 0.1	7.8 ± 3.1

Final density ρ, orientation degree I_{200}/I_{002}, mean grain size D; aspect ratio a of elongated Si_3N_4 grains.
(*) I_{200}/I_{002} relative to a random orientation: 6.6.

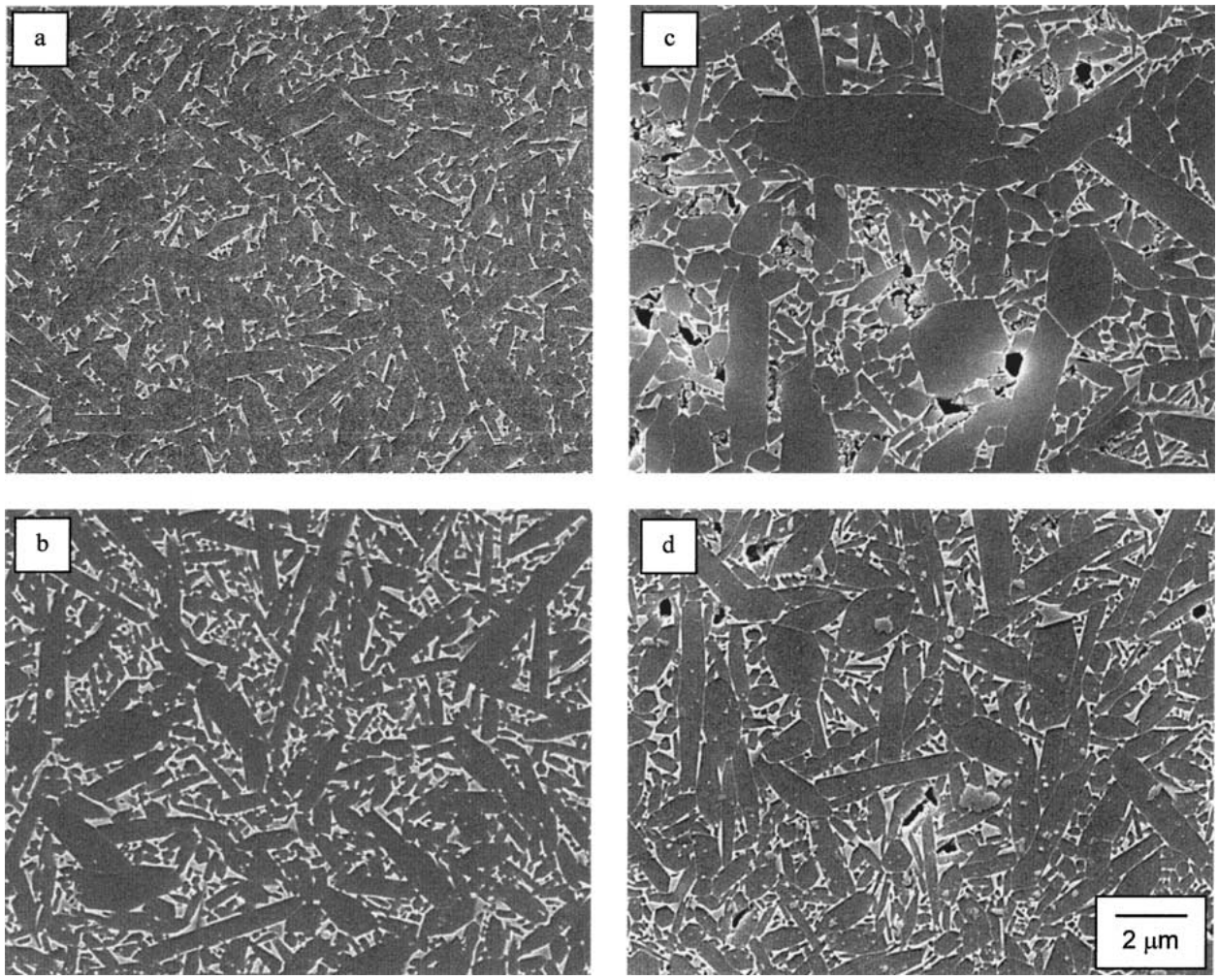

Figure 5 SEM micrographs of polished and plasma etched surfaces (perpendicular to the applied pressure) from materials obtained by ultrasonic dispersed mixtures: 1 Uu (a), 1 Bu (b), 1 Pu (c), and 1 Mu (d).

(Fig. 7a and b). Materials from powder U reached full density and showed only negligible microporosity. Samples from powder M and P presented some pores and poorly dense areas (Fig. 5c and d). The use of powder U, both processed by ultrasonic mixing or chemical coprecipitation, offers the more uniform *in situ* composite microstructure with the highest aspect ratio and the lowest grain size. High additive content favours, in composition 2, the development of finer grains with aspect ratio up to about $\sim$10, particularly in the sample obtained by chemical coprecipitation.

Materials from powder B, although nearly fully dense, have inhomogeneities: abnormal grains were revealed in sample from the coprecipitated powder. The origin of these defects is therefore dependent on the powder processing procedure.

Materials from powder P have evident microstructural inhomogeneities (i.e. low dense areas, pores).

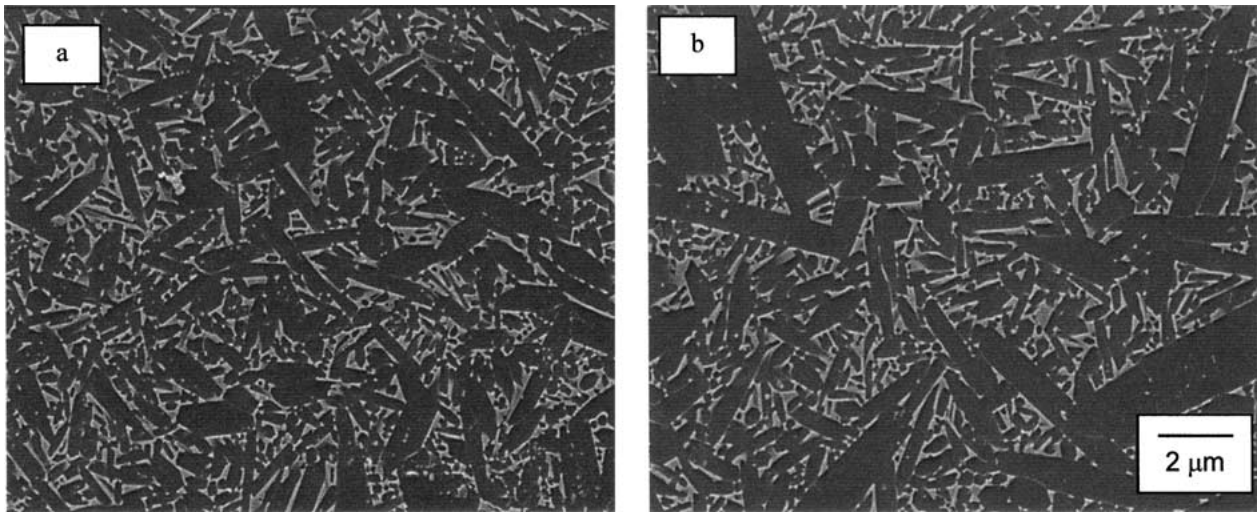

Figure 6 SEM micrographs of polished and plasma etched surface (perpendicular to the applied pressure during hot pressing) from Si_3N_4 powder B and composition 1: (a) ultrasonic dispersed mixtures and (b) coprecipitated mixtures.

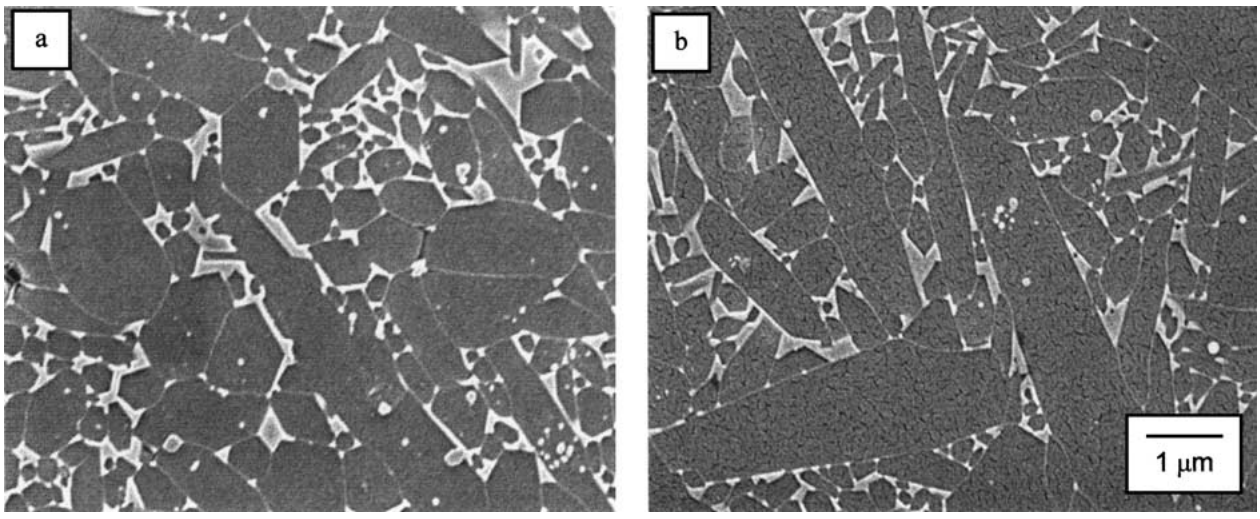

Figure 7 SEM micrographs from polished and plasma etched surface of sample 1 Mu, parallel (a) and perpendicular (b) to the direction of applied pressure during hot pressing.

These features are due to characteristics of the starting powder P: the wide particle size distribution and the low surface reactivity, that prevent the formation of a homogeneous coating of particles with additives. These factors implied low sinterability and the achievement of poorly dense samples. The high content of impurities in the starting powder lowered the liquidus temperature, favoured the growth of grains with lower aspect ratio and less homogeneous final microstructure (Fig. 5c). Moreover, the carbon contamination of the powder (Tables I and II) could have locally impoverished the liquid phase, through the formation of carbide volatile species [33]. All these factors justify, particularly when additive powders were introduced by ultrasonic mixing, the worst results obtained with powder P, among the four tested powders.

Samples from powder M, particularly the coprecipitated mixture, reached satisfactory final density with a rather coarse microstructure.

All the above-described microstructural features depend mainly on the additive system and oxygen plus other impurities that lower the liquidus temperature. In fact, M and P powders evidence a liquidus temperature 200°C lower than powder U. Generally more oxygen in chemically processed mixtures lowers the liquidus temperature in respect with those from ultrasonic mixing. Considering that the viscosity of the liquid phase is proportional to the temperature of the liquid formation, densification and grain growth kinetics are different for the various samples, being the diffusion coefficients reversely related to the viscosity of the liquid phase [1, 34]. The experimental data evidence a reverse relationship between liquidus temperature and mean grain size. A more viscous medium limits mass transport, this retards grain growth and favours the development of fine and fibrous microstructure: it was experimentally confirmed by the behaviour of samples 1U and 2U containing two different amounts of additives. Composition 2 in fact (due to the scarce influence of powder impurities) presented the higher liquidus temperature and the final lower mean grain size, associated with the highest aspect ratio.

In the hot pressed materials, no crystalline grain boundary phases were detected on X-ray spectra, except in Bu sample, where traces of Y-La-silicates were found. These species probably derive from the higher

amount of oxygen in the starting B powder. After annealing tests at 1400°C for 6 hours, amounts from 2 to 6 vol% of crystalline phases (La-Y-Si-O-N and La-Si-O phases with various stoichiometries) were revealed.

The presence of different grain boundary phases in the various samples was confirmed by thermal expansion tests. In fact, heating up (5°C/min) the test samples, two devitrification humps generally occurred, the former in the temperature range 1000–1200°C and the latter 1250–1400°C, being attributable respectively to the devitrification of glassy silicates and oxynitrides. Some studies [35–38] reported that the substitution of nitrogen for oxygen in the glass network produces a more rigid network increasing the viscosity of the glass. The transition temperature of these glasses increases with nitrogen content and with the type of the network modifier: amorphous phases in the system La-Y-Si-O-N have transition temperatures higher of about 200°C in respect with other oxynitrides [36–38]. Therefore, due to the selected additives ($Y_2O_3 + La_2O_3$), the high coordination number of La^{3+} and Y^{3+} as glass modifiers is also beneficial for a more rigid glass network in comparison to the action of other cations.

5. Mechanical properties

With reference to the values of the tested mechanical properties (Table VI), the relationship between properties and microstructure is discussed below.

5.1. Young's modulus (E)

Residual porosity is the primary factor influencing E. The E values of the nearly full dense samples range from 322 to 329 GPa. These values are higher than those generally found for silicon nitride produced with other sintering aids [1, 4, 16]. It may be ascribed to the characteristics of the residual grain boundary phases: less sintering aids and stiffer residual Y-La-oxynitride glasses [4, 36]. The lower value from sample Bu is probably due to the higher amount of glassy or crystalline silicates in the intergranular phases.

5.2. Hardness (HV1.0)

Because of the residual porosity, larger grain size and other microstructural defects, samples from powder P and M were less hard than those from powder U and B. The hardness measured on the surface perpendicular to the applied pressure during sintering is higher than that in the surface parallel. This accounts for the anisotropic microstructure after sintering.

5.3. Toughness and crack propagation

In all the produced materials, a toughening effect arises from a combination of factors like number, size and aspect ratio of textured β-Si_3N_4 grains, as evidenced from tests in two perpendicular directions (Table VI and Fig. 8a and b). In the surface perpendicular to the

TABLE VI Mechanical properties of the hot pressed materials

		HV1.0 (GPa)		K_{IC} (MPa$\sqrt{m}$)		σ (MPa)			
Sample	E (GPa)	//	⊥	//	⊥	RT	1000°C	1200°C	1400°C
1 Uc	329	17.2 ± 0.4	18.4 ± 0.8	4.6 ± 0.1	5.8 ± 0.2	990 ± 142	751 ± 76	746 ± 85	735 ± 53
1 Uu	325	17.8 ± 0.5	18.2 ± 0.6	4.3 ± 0.1	5.7 ± 0.2	1137 ± 65	889 ± 99	789 ± 32	678 ± 57
1 Bc	323	16.5 ± 0.7	17.4 ± 0.9	3.8 ± 0.1	4.1 ± 0.4	695 ± 48	612 ± 58	544 ± 27	494 ± 43
1 Bu	317	17.0 ± 0.6	18.5 ± 0.9	3.7 ± 0.4	4.1 ± 0.1	619 ± 173	677 ± 23	593 ± 33	521 ± 10
1 Pc	304	15.4 ± 0.7	15.3 ± 0.9	3.8 ± 0.1	4.7 ± 0.2	841 ± 62	622 ± 58	571 ± 45	473 ± 27
1 Pu	282	11.4 ± 0.9	15.0 ± 1.2	5.5 ± 0.4	5.2 ± 0.4	583 ± 20			
1 Mc	322	17.1 ± 0.5	17.8 ± 0.4	4.4 ± 0.3	5.1 ± 0.3	786 ± 74	582 ± 70	399 ± 28	
1 Mu	328	14.7 ± 0.6	16.1 ± 0.7	5.0 ± 0.4	5.6 ± 0.4	694 ± 74	594 ± 57	393 ± 26	
2 Uu	325	17.5 ± 0.4	18.9 ± 0.3	4.9 ± 0.2	5.7 ± 0.1	941 ± 67	826 ± 29	974 ± 71	771 ± 56
2 Uc	325	17.1 ± 0.5	18.1 ± 0.5	5.0 ± 0.3	5.5 ± 0.1	941 ± 84	927 ± 52	968 ± 30	761 ± 32

Young's modulus E, Vicker's hardness HV1.0, fracture toughness K_{IC}, flexural strength σ at various temperatures.

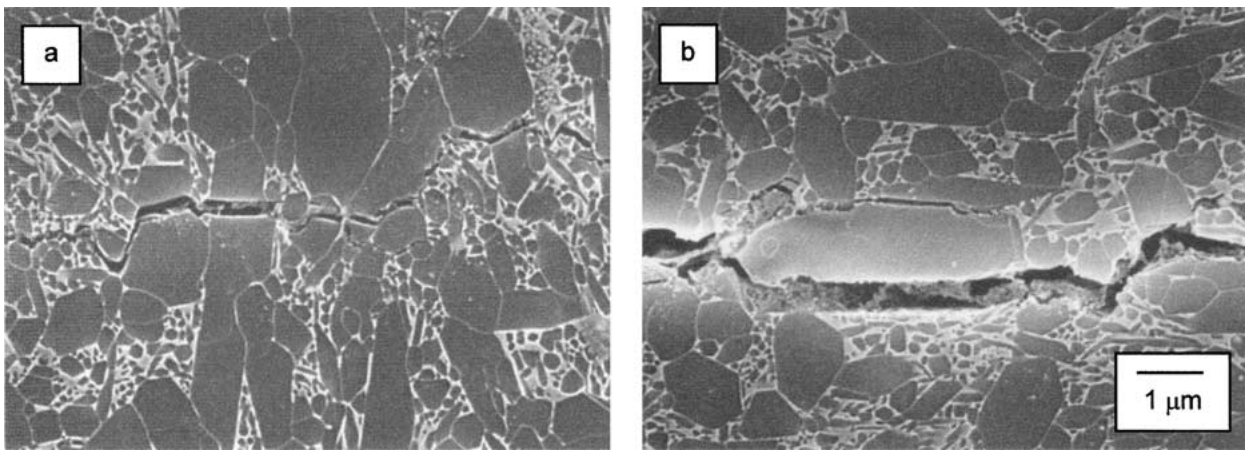

Figure 8 Comparison of the crack propagation on a surface parallel to the applied pressure: (a) shorter crack and (b) longer crack.

hot press direction, a larger number of rod-like β-Si_3N_4 grains with crystallographic c-axis lying upon this surface favours the crack deflection along grain boundaries and, sometimes, the bridging of the advancing crack. These mechanisms reduce the constraint level on the crack tip toughening the material.

Crack deflection was more frequently observed in samples with aspect ratio higher than 7 and/or is more pronounced in materials with larger grain size.

5.4. Room temperature flexural strength

The flexural strength values were found to vary significantly (Table VI). Excellent values (in the range 900–1200 MPa) were recorded only in samples produced with powder U, particularly in composition 1. Slight difference can be associated to the powder processing route. It means that, after an effective dispersion of additives, fine and pure raw silicon nitride powder strongly limits detrimental effects on service of the defect population. Among the nearly full dense samples, the lowest strength concerns samples from powder B that, although "fine and pure", come from a raw powder with acid surfaces, which limit a uniform coating of the powder surface with additives. The more frequently observed defects, in fact, are due to the poor homogeneity of the grain boundary phases. The presence of coarse particles in the starting powders P and M and the lacking homogeneity in the distribution of the additives can explain the development of microstructural defects like exaggerated grains associated to poorly dense areas (an example is shown in Fig. 9).

5.5. Flexural strength at high temperatures

In addition to the manufacturing defects and the relaxation of machining residual stresses, the softening of the grain boundary phases and the introduction of new flaws (i.e. oxidation pits) represent the main features that affect and degrade strength at high temperatures in air.

Materials from powder U showed remarkable performances up to 1400°C with strength values near to about 800 MPa. Sample 1Uc shows a constant strength from 1000 to 1400°C, samples 2Uc and 2Uu from room temperature to 1200°C, accompanied by a slight decrease at 1400°C (18%). It confirms the effectiveness of the selected additive system to yield highly refractory grain boundary phases for the development of high performance materials at high temperatures. Samples from powder B maintain rather good strength up to 1400°C.

Materials produced with powder P and particularly M show a significant strength decrease at 1200°C, where the values are about half of those measured in samples from powder U. The strength decrease is related to less refractory grain boundary phases, confirming the above discussed assessment on the relationships among impurities—liquid phase characteristics during sintering—grain boundary phase refractoriness in the dense silicon nitrides.

Another important factor is the distribution of grain boundary phases. The coarser is the microstructure, the larger are the glassy pockets at triple grain junctions: failure can originate there under stresses and then advance along the grain boundary layer. It can be a feature influencing in particular samples P and M with coarser microstructure.

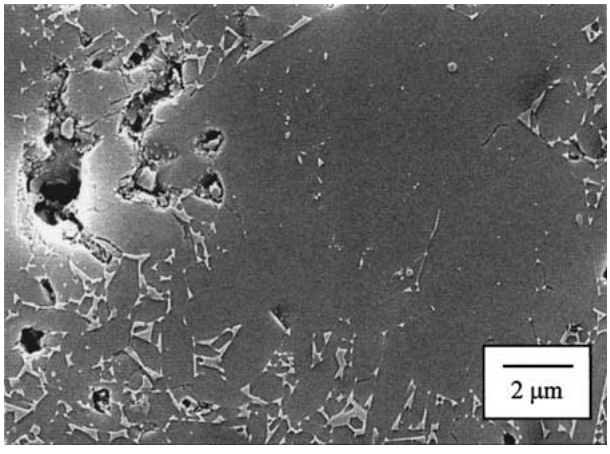

Figure 9 SEM micrograph of polished and plasma etched surface from sample 1 Pc: abnormal grains and poorly dense areas are shown.

6. Conclusions

Starting from four commercial silicon nitride powders, two processing routes (ultrasonic mixing and chemical coprecipitation) were developed for the addition of sintering aids ($Y_2O_3 + La_2O_3$). Relationships among characteristics of the starting powders, processing methods, sintering behaviour under hot pressing were investigated.

The different powder processing routes gave rise to similar surface layer composition of the additive species but to different layer morphologies and screening effects. The generally superior qualities of powder U assure a homogeneous and complete superficial covering of additives that results in a better sinterability of the mixed powder, in respect to powder mixtures from the other Si_3N_4 powders.

A fibrous microstructure of hot pressed silicon nitride was obtained, however grain size, aspect ratio, microstructural homogeneity and characteristics of the grain boundary phases depend on powder characteristics and powder processing routes. In particular the more uniform coating of Si_3N_4 powder particles with additive species reflects the best performances of the powder mixture in terms of sinterability and resulting microstructure, as observed in materials from powder U. In the case of the other powders (B, P, M), for both the powder processing routes, several concurrent factors such as broad grain size distribution, impurity content and high content of SiO_2 species upon the particle surface affect microstructure.

The observed microstructural characteristics induce specific effects on mechanical properties. The measured mechanical properties highlight the merit of the silicon nitride powders produced by chemical syntesis (U and B) in respect with the powders from nitridation of silicon (P and M). The highest strengths (950–1200 MPa at room temperature and 700–800 MPa at 1400°C) were measured on samples from powder U for both the sintering aid amounts and rather independently on the procedure adopted to introduce sintering aids. Materials

from powder B, although their strength are quite lower (600–800 MPa at room temperature and about 500 MPa at 1400°C) can be still considered satisfactorily with a limited strength degradation.

On the contrary the strength of materials from powders P and M decreases at 1200°C to values about half of those measured on samples from powder U. This is due to a less refractory secondary phase, as a consequence of metal impurities in the starting powders and to a wide grain size distributions.

Comparing the procedures adopted for the addition of the sintering aids, no significant differences in terms of resulting mechanical properties can be evidenced. Concerning the chemical route, further improvements can be gained from a more rigorous control of the experimental parameters, provided that the powders are pure, fine and with a controlled acidic surface. If the additives are powders, further benefits remain difficult, because of the finite size of the particles.

For these reasons, ultrasonic processing is favoured as a fast, clean, cheap and efficient route. It does not require the use of expensive precursors or equipments and time-consuming processing like the chemical coprecipitation.

The results make it clear that grain size distribution and surface species of the starting powder are the key factors for the production of high performance silicon nitride, but a strict control of the powder treatments and the design of sintering aid systems remain as requisites.

Acknowledgements

The authors wish to thank Dr. F. Bertoni, Mr. D. Dalle Fabbriche (IRTEC-CNR) for the technical assistance, Dr. P. Traverso (ICMM-CNR) for XPS analyses, Dr. S. Guicciardi and Mr. C. Melandri for their skillful collaboration in the measurements of mechanical properties.

References

1. G. WOTTING and G. ZIEGLER, *Ceram. Intern.* **10** (1984) 18.
2. H. J. KLEEBE and G. ZIEGLER, *J. Amer. Ceram. Soc.* **72** (1989) 2314.
3. C. GALASSI, V. BIASINI and A. BELLOSI, *Processing of Adv. Mater.* **3** (1993) 153.
4. A. BELLOSI, F. MONTEVERDE and G. N. BABINI, in "Engineering Ceramics '96, High Reliability Through Processing," edited by G. N. Babini, M. Haviar and P. Sajgalik, NATO ASI Series Vol. 25, (Kluwer Acad. Publ., Dordrecht, 1997) p. 197.
5. T. M. SHAW and B. A. PETHICA, *J. Amer. Ceram. Soc.* **62** (1986) 88.
6. G. RIEDEL, H. BESTGEN and M. HERMANN, *CFI/DKG* **75** (1999) 24.
7. S. KANZAKI, M. E. BRITO, M. C. VALECILLOS, K. HIRAO and M. TORIYAMA, *J. Europ. Ceram. Soc.* **17** (1997) 1841.
8. L. WANG, W. M. SIGMUND, S. ROY and F. ALDINGER, *J. Mater. Res.* **14** (1999) 4562.
9. H. BJORKLUND, L. K. L. FALK, K. RUNDGREN and J. WASEN, *J. Europ. Ceram. Soc.* **17** (1997) 1285.
10. D. S. PERERA, DE. R. G. MITCHELL and S. LEUNG, *ibid.* **20** (2000) 789.
11. J. S. KIM, H. SHUBERT and G. PETZOW, *ibid.* **5** (1989) 311.
12. M. WANG and F. L. RILEY, *Am. Ceram. Soc. Bull.* **10** (1992) 83.
13. P. N. JOSHI and R. A. McCAULEY, *J. Amer. Ceram. Soc.* **77** (1994) 2926.
14. H. SCHMIDT, G. NABERT, G. ZIEGLER and H. GOREZKI, *J. Europ. Ceram. Soc.* **15** (1995) 667.
15. H. J. KLEEBE, W. BRAUE, H. SCHMIDT, G. PEZZOTTI and G. ZIEGLER, *ibid.* **16** (1996) 339.
16. A. BELLOSI and G. N. BABINI, in "Key Engineering Materials," Vols. 161–163, edited by K. Niihara, T. Sekino, E. Yasuda and T. Sasa (Trans Tech. Publ., Vetikon, Switzerland, 1999) p. 203.
17. M. KULIG and P. GREIL, *J. Mater. Sci.* **26** (1991) 216.
18. S. G. MALGHAN, V. A. HACKLEY and P. S. WANG, in "Ceramic Engineering and Scientific Processing" (American Ceramic Society, Westerville, OH, 1994) p. 527.
19. C. GALASSI, F. BERTONI, S. ARDIZZONE and L. C. BIANCHI, *J. Mater. Res.* **15** (2000) 155.
20. *Idem.*, *J. Amer. Ceram. Soc.* **82** (1999) 2653.
21. C. GALASSI, E. RASTELLI, E. RONCARI, S. ARDIZZONE and M. G. CATTANIA, *J. Mater. Res.* **10** (1995) 339.
22. ASTM C 848-78 (Reapproved 1983)
23. G. R. ANSTIS, P. CHANTIKUL, B. R. LAWN and D. B. MARSHALL, *J. Amer. Ceram Soc.* **64** (1981) 533.
24. J. F. MOULDER, W. F. STICKLE and K. D. BOMBEN, "Handbook of X-ray Photoelectron Spectroscopy" (Perkin Elmer Corporation, Eden Praire, MN, 1992).
25. S. M. CASTANHO, J. L. G. FIERRO and R. MORENO, *J. Europ. Ceram Soc.* **17** (1997) 383.
26. S. M. CASTANHO, R. MORENO and J. L. G. FIERRO, *J. Mater. Sci.* **32** (1997) 157.
27. E. LYDEN, L. BERGSTROM, M. PERSSON and R. CARLSSON, *J. Europ. Ceram. Soc.* **7** (1991) 361.
28. M. STRAUSS, T. RING, A. BLEIER and H. K. BOWEN, *J. Appl. Phys.* **58** (1963) 3871.
29. A. BELLOSI and G. N. BABINI, in "Key Engineering Materials, 89-91, Silicon Nitride'93," edited by M. J. Hoffmann, P. F. Becher and G. Petzow (Trans Tech. Publ., Aedermannsdorf, Switzerland, 1994) p. 117.
30. E. M. LEVIN and H. F. Mc. MURDIE, "Phase Diagrams for Ceramists," edited by M. K. Reser (The American Ceramic Society, Inc. Columbus, OH, 1975) p. 153.
31. E. M. LEVIN, C. R. ROBBINS and H. F. McMURDIE, "Phase Diagrams for Ceramists," edited by M. K. Reser (The American Ceramic Society, Columbus, OH, 1969) p. 153, p. 167.
32. W. D. KINGERY, J. M. WOULBROUN and F. R. CHARVAT, *J. Amer. Ceram. Soc.* **746** (1963) 391.
33. H. LANGE, G. WOETTING and G. WINTER, *Angewandte Chemie* **103** (1981) 1606.
34. S. HAMPSHIRE, in "Materials Science and Technology," Vol. 11, edited by R. W. Cahn, P. Haasen and E. J. Kramer (VCH, Weinheim, 1994) p. 119.
35. J. CHEN, P. WEI and Y. HUANG, *J. Mater. Sci Lett.* **16** (1977) 1486.
36. S. HAMPSHIRE, R. A. L. DREW and K. H. JACK, *Comm. Am. Cer. Soc.* (1984) C-46.
37. R. E. LOEHMAN, *J. Non-Cryst. Solids* **56** (1983) 123.
38. T. M. SHOW, G. THOMAS and R. E. LOEHMAN, *J. Amer. Ceram. Soc.* **67** (1984) 643.

Received 14 December 2000
and accepted 6 June 2001